SIMULTANEOUS MICROFLUIDIC SYNTHESIS AND SILANIZATION OF IRON OXIDE NANOPARTICLES

Adelina-Gabriela NICULESCU [1,2], Alexandra Cătălina BÎRCĂ [1], Alina MOROȘAN [3], Ovidiu Cristian OPREA [4], Bogdan Ștefan VASILE [5,6], Bogdan PURCĂREANU [1,7], Dan Eduard MIHAIESCU [8], Alexandru Mihai GRUMEZESCU [9,10]

Iron oxide nanoparticles (Fe_3O_4 NPs) have garnered significant attention in recent years due to their favorable physicochemical and biological characteristics, which make them highly versatile for various applications. As a result, there is an increasing focus on optimizing synthesis approaches to ensure they are both more efficient and reproducible. Thus, this study proposes utilizing emerging microfluidic technologies to fabricate uniform core (Fe_3O_4)-shell (3-aminopropyltriethoxysilane - APTES) NPs with tunable characteristics, accomplishing the material's simultaneous on-chip synthesis and silanization within a 3D microfluidic platform. The synthesized nanomaterials were analyzed using several techniques, including XRD, FT-IR, DLS, TEM, and TG-DSC techniques.

Keywords: microfluidic synthesis; on-chip functionalization; 3D microfluidic platform; iron oxide nanoparticles; organosilane shell

[1] Ph.D. student, Dept. of Science and Engineering of Oxide Materials and Nanomaterials, National University of Science and Technology POLITEHNICA Bucharest, Romania, e-mail: adelina.niculescu@upb.ro, ada_birca@yahoo.com, bogdanpb89@gmail.com

[2] ACS, ICUB—Research Institute of the University of Bucharest, Romania, e-mail: adelina.niculescu@upb.ro

[3] Assist. Prof., Dept. of Organic Chemistry, National University of Science and Technology POLITEHNICA Bucharest, Romania, e-mail: alina.morosan@upb.ro

[4] Prof., Dept. of Inorganic Chemistry, National University of Science and Technology POLITEHNICA Bucharest, e-mail: ovidiu.oprea@upb.ro

[5] CS II., National Research Center for Micro and Nanomaterials, National University of Science and Technology POLITEHNICA Bucharest, Romania, e-mail: bogdan.vasile@upb.ro

[6] CS II., Research Center for Advanced Materials, Products and Processes, National University of Science and Technology POLITEHNICA Bucharest, Romania, e-mail: bogdan.vasile@upb.ro

[7] Eng., BIOTEHNOS SA, Otopeni, Romania, e-mail: bogdanpb89@gmail.com

[8] Prof., Dept. of Organic Chemistry, National University of Science and Technology POLITEHNICA Bucharest, Romania, e-mail: danedmih@gmail.com

[9] Prof., Dept. of Science and Engineering of Oxide Materials and Nanomaterials, National University of Science and Technology POLITEHNICA Bucharest, Romania, e-mail: agrumezescu@upb.ro

[10] CS I, ICUB—Research Institute of the University of Bucharest, Romania, e-mail: agrumezescu@upb.ro

1. Introduction

Nanomaterials are recognized for their valuable properties related to characteristic small sizes, fine-tuned morphologies, crystalline structure, adaptable chemical composition and charge, and improved solubility, which recommend them for a wide range of applications [1-6]. Metal oxide nanoparticles are among the most utilized exponents of nanotechnology, being applied as catalysts, nanocarriers, water treatment solutions, textile enhancers, and functionalization materials in polymer composites, adhesives, and coatings [7]. Magnetic nanoparticles, in particular, are gaining increasing interest in numerous and varied technological areas, being acknowledged for their low prices, enhanced biocompatibility, good chemical stability, and size-dependent magnetic activity [8,9].

Magnetite (Fe_3O_4) has been especially remarked among promising magnetic nanoparticles due to the high versatility of this nanomaterial, its wide availability, eco-friendliness, and superparamagnetic behavior [10,11]. However, Fe_3O_4 nanoparticles have a high surface energy (that causes their agglomeration in ionic solutions) and present a lack of affinity for biomolecules. To overcome these drawbacks, Fe_3O_4 nanoparticles are generally functionalized or surface-modified with different compounds [10-12]. Silanes are extensively used as bifunctional modifiers to alter the surface chemistry of metal oxide nanoparticles. Among these, 3-aminopropyltriethoxysilane (APTES) is particularly effective in functionalizing Fe_3O_4 nanoparticles, helping to prevent their agglomeration through steric repulsion. Moreover, the terminal amine group in APTES enables further bioconjugation or serves as a bridge in the synthesis of composite or hybrid structures, facilitating the integration of Fe_3O_4 nanoparticles with other inorganic materials or allowing additional functionalization with organic molecules such as peptides, antibodies, oligonucleotides, or polymers [7,12,13].

Concerning synthesis methods, Lab-on-a-Chip (LoC) devices represent a revolutionary approach in nanotechnology, enabling nanoparticle production with narrow size distribution and uniform morphology. Microfluidic platforms offer a restrained and reproducible environment that allows precise operating parameter modifications, tailored mixing dictated by controlled flow rate and reaction time, and significant reduction of reagent consumption and waste generation, all these characteristics rendering them suitable for the eco-friendly obtaining of nanoparticles with fine-tuned composition, structure, and physicochemical properties [2,13-21]. Moreover, microreactors benefit from mitigating or eliminating possible human errors, leading to considerably reduced batch-to-batch variability and more time-efficient synthesis routes [13,22].

In this context, microfluidic platforms have been explored, with various systems reported for the on-chip synthesis of Fe_3O_4 nanoparticles. However, most

current microreactors primarily utilize two-dimensional mixing strategies, while microfluidic 3D mixing is still in its nascent stages of development. Shifting from traditional planar geometries to three-dimensional micromixers holds considerable promise for advancing microfluidic technology. The incorporation of a third dimension in fluid manipulation extends contact times between fluids, disrupts surface flow, and reduces channel length, all of which contribute to more efficient mixing [20,23].

Therefore, this study aims to explore the potential of a new custom-made 3D microfluidic platform for fabricating uniform core-shell Fe_3O_4-APTES nanoparticles with well-controlled dimensional and morphological characteristics. The synthesis process involves a one-step microfluidic-assisted co-precipitation and functionalization reaction, confined within the channels of a multilayered system. To verify the successful synthesis of the target materials, characterization was performed using XRD, FT-IR, DLS, TEM, and TG-DSC techniques.

2. Experimental part

2.1. Materials

Ferric chloride ($FeCl_3$), iron sulfate heptahydrate ($FeSO_4 \cdot 7H_2O$), and 3-aminopropyltriethoxysilane (APTES) were sourced from Sigma Aldrich Merck (Darmstadt, Germany), while sodium hydroxide (NaOH) was acquired from Lach-Ner (Tovarni, Czech Republic). All reagents were of analytical grade and utilized directly without any additional purification steps.

2.2. Nanoparticle preparation

A precursor solution was prepared by dissolving 1.5 g of $FeCl_3$ and 9 g of $FeSO_4 \cdot 7H_2O$ in 900 mL of ultrapure water, while the precipitating solution consisted of 45 g of NaOH dissolved in 900 mL of ultrapure water. The iron oxide nanoparticles were synthesized through co-precipitation, initiated by the interaction of iron ions with the alkaline solution. Both reagent solutions were introduced simultaneously into the microfluidic setup, as described in a previous study [13], allowing the reaction to occur within a multipoint three-dimensional mixing system (Fig. 1).

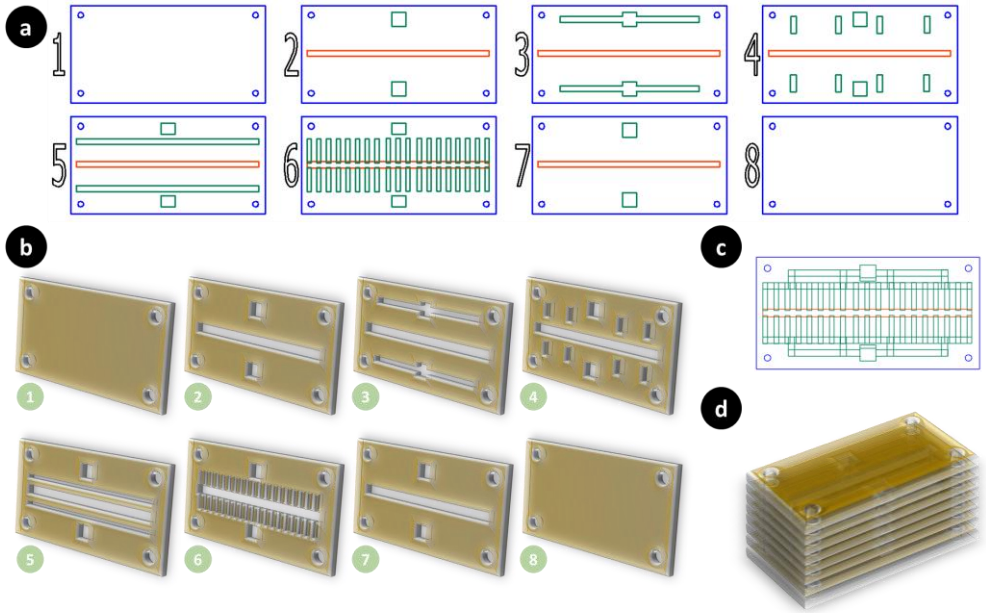

Fig. 1. Microfluidic platform configuration includes: (a) proportional 2D and (b) 3D schematic depictions of the individual layers of the platform, as well as (c) 2D and (d) 3D overlayed views of the entire microfluidic device. Adaptation of the figure published by authors in an open-access article [13].

The same procedure was employed to synthesize the functionalized nanoparticles, with the addition of 4 mL of APTES to the iron precursor solution. The resulting nanoparticles were subsequently subjected to multiple washing cycles with ultrapure water, followed by ultrasonication and centrifugation, to remove any residual unreacted chemicals.

2.3. Characterization methods

2.3.1. XRD

XRD analysis was performed using a Panalytical Empyrean diffractometer (PANalytical, Almelo, The Netherlands) equipped with a CuKα radiation source (λ = 1.056 Å). The nanomaterial powders were scanned at 40 mA and 45 kV, covering a Bragg diffraction angle range of 10° to 80°. Measurements were conducted at room temperature with an incidence angle of ω = 0.5°.

2.3.2. FT-IR

The synthesized nanostructures were analyzed using a Nicolet iS50 FT-IR spectrometer (Thermo Fisher Scientific, Waltham, Massachusetts, USA). The measurements were performed at room temperature, spanning a spectral range of 4000–400 cm^{-1} with a resolution of 8 cm^{-1}. All spectra were recorded in

attenuated total reflectance (ATR) mode, utilizing a diamond crystal. For each sample, 96 scans were collected, co-added, and processed using Omnic 8.2.0 software (Thermo Fisher Scientific).

2.3.3. DLS

DLS measurements were carried out on the synthesized nanomaterials as follows: the nanoparticles were first dispersed in water and then sonicated for 5 minutes, followed by a transfer to the cuvettes of a Nano ZS Zetasizer (Malvern Instruments, Malvern, UK). The measurements were taken at a scattering angle of 90° and a temperature of 25 °C.

2.3.4. TEM

For TEM analysis, the nanomaterials were dispersed in ethanol and subjected to 15 minutes of ultrasonic treatment. A small volume of the dispersion was then dropped onto a 400-mesh lacey carbon-coated copper grid and allowed to air-dry at room temperature. High-resolution TEM micrographs were obtained using an 80–200 Titan Themis transmission electron microscope (ThermoFisher Scientific, Hillsboro, OR, USA), operated at 200 kV in transmission mode, with point and line resolutions of 2 Å and 1 Å, respectively. Crystallographic information was further provided by the SAED accessory of the microscope.

2.3.5. TG-DSC

TG-DSC analyses were conducted using an STA 449C Jupiter device (NETZSCH-Gerätebau GmbH, Selb, Germany). A small amount of the sample was placed in an open alumina crucible and heated at a constant rate of 10°C per minute, from ambient temperature to 900°C. The analysis took place under a dry airflow of 50 mL per minute, with an empty alumina crucible used as a reference. Furthermore, the gases released during the process were analyzed using an FTIR Tensor 27 spectrometer (Bruker Co., Ettlingen, Germany), equipped with a thermostat-regulated gas cell.

3. Results and discussion

The XRD analysis results are presented in Fig. 2. Distinctive diffraction peaks corresponding to Fe_3O_4 were observed in both the pristine and APTES-modified nanoparticles. The diffraction planes (220), (311), (400), (422), (511), and (440) were observed, which, based on JCPDS 01-084-2782, correspond to crystalline magnetite with a cubic spinel structure. It was also noted that the diffraction peaks for the Fe_3O_4@APTES nanoparticles were less pronounced compared to the unmodified material, exhibiting reduced heights and slightly broader widths.

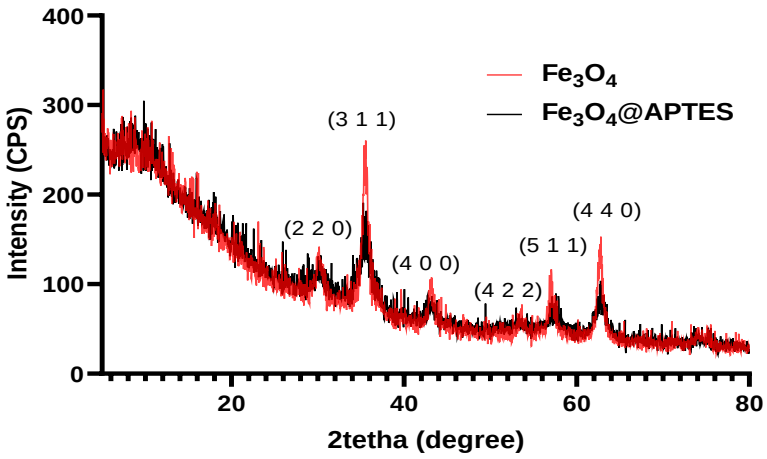

Fig. 2. X-ray diffractograms of pristine Fe_3O_4NPs and Fe_3O_4@APTES NPs.

The successful functionalization of nanoparticles with APTES was further confirmed by FT-IR analysis, as shown in Fig. 3. Both sample spectra showed characteristic features of hydroxyl groups, with a broad absorption band around 3400 cm^{-1} corresponding to O-H stretching vibrations, and a smaller peak near 1630 cm^{-1}, related to O-H bending vibrations. Additionally, both materials exhibited the expected adsorption bands for Fe-O stretching vibrations, observed at 542 cm^{-1} and 543 cm^{-1} for pristine Fe_3O_4 and Fe_3O_4@APTES, respectively. A key difference between the spectra is the presence of broad peaks at 3350 cm^{-1} and 3247 cm^{-1} in the surface-modified sample, which are attributed to N-H stretching vibrations. The amino group is also indicated by the peak at 1539 cm^{-1}, corresponding to N-H bending vibrations. Furthermore, the absorption bands at 2975 cm^{-1} and 2928 cm^{-1} provide additional evidence of nanoparticle silanization, confirming the presence of APTES [24-26].

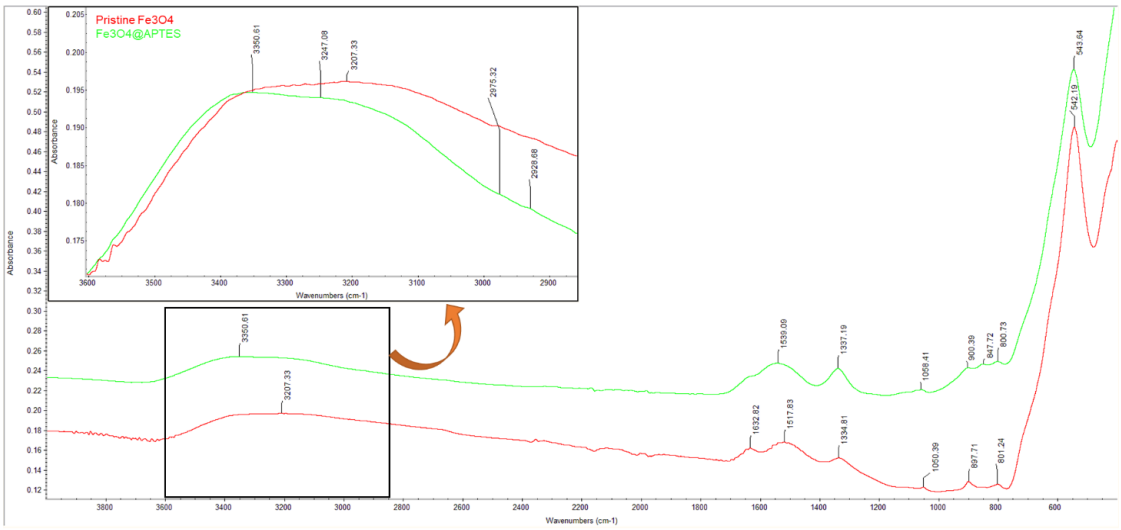

Fig. 3. Comparison between FT-IR spectra of pristine Fe_3O_4 and Fe_3O_4@APTES NPs.

The obtained materials were also compared from the points of view of their size and colloidal stability, with Table 1 and Fig. 4. summarizing DLS results. Pristine Fe_3O_4 nanoparticles exhibited an average hydrodynamic diameter of approximately 52 nm and a polydispersity index of 0.167, both of which increased upon functionalization. Having a higher hydrodynamic diameter (i.e., ~128 nm) for Fe_3O_4@APTES NPs is an expected result, given the additional shell covering the magnetic core of the particles subsequent to silanization. The increase in polydispersity may be attributed to the bi-modal size distribution observed for these nanoparticles, which is in contrast to the clear single peak obtained for unmodified magnetite. Nonetheless, these findings are consistent with our previous research, where functionalization under microwave irradiation has also broadened the size distribution [13]. The high absolute values obtained for the Zeta potential reflect the high stability of the analyzed dispersions, being within the characteristic range for metal oxide nanoparticles [27]. In more detail, having high Zeta potentials, the fabricated nanostructures exhibit a strong enough double-layer repulsion effect that prevents their aggregation [28].

Table 1

Characteristics of synthesized NPs determined by DLS analyses.

Nanoparticle type	Average hydrodynamic diameter (nm)	Polydispersity index	Zeta potential (mV)
Pristine Fe_3O_4 NPs	51.81	0.167	-54.9
Fe_3O_4@APTES NPs	127.6	0.244	-45.4

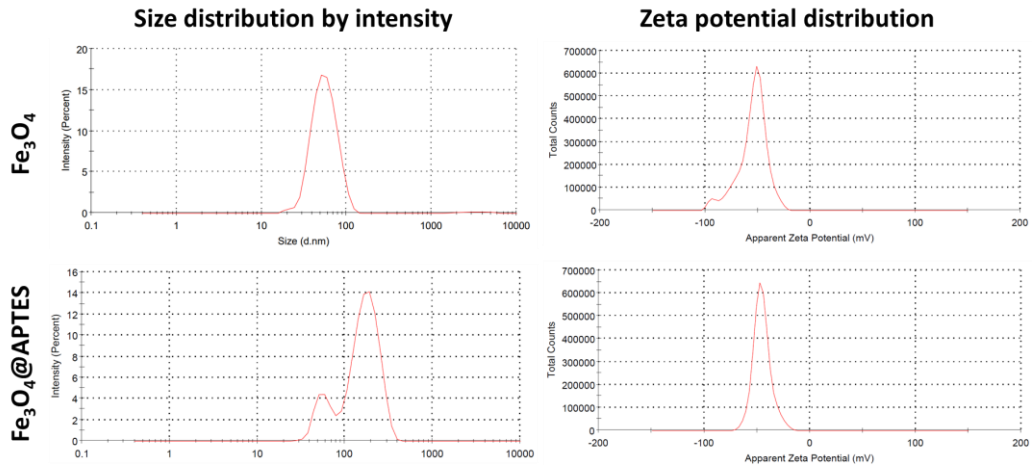

Fig. 4. Size distribution and Zeta potential distribution of pristine Fe_3O_4 and Fe_3O_4@APTES NPs.

TEM micrographs enabled detailed visualization of the fabricated nanomaterials, providing insights into their morpho-structural properties. The analysis of pristine Fe_3O_4 nanoparticles showed the formation of uniform particles with a predominantly spherical shape and minimal aggregation (Fig. 5.a). The HR-TEM image (Fig. 5.b) further revealed the presence of ultra-small particles coated with an outer dispersant layer. Additionally, SAED analysis of the unmodified magnetite nanoparticles (Fig. 5.c) showed six concentric rings corresponding to the (220), (311), (400), (422), (511), and (440) diffraction planes. These findings are consistent with the XRD data, further confirming the crystallinity of the analyzed material.

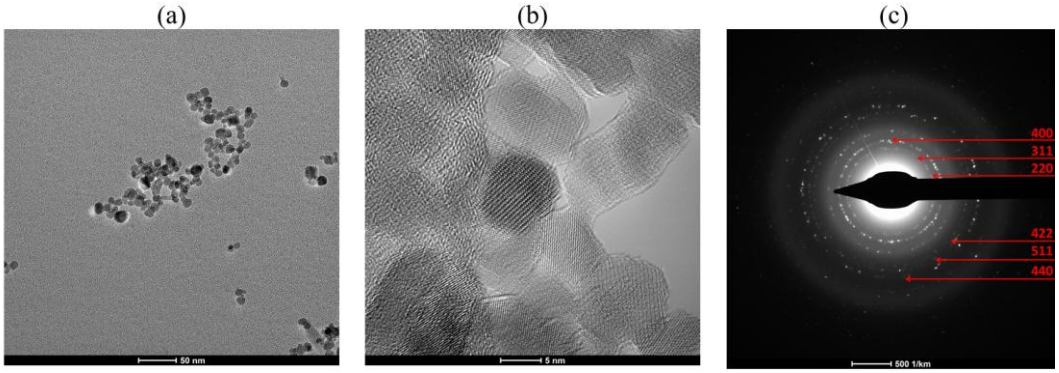

Fig. 5. Pristine Fe_3O_4 NPs: (a) TEM and (b) HR-TEM micrographs, and (c) SAED diffraction pattern with the corresponding Miller indices.

In contrast, TEM images obtained for Fe_3O_4@APTES NPs (data not shown) revealed an increase in particle size attributed to the silica shell covering

the magnetic cores. The functionalized nanomaterials were also uniform in size and morphology and exhibited the characteristic rings for magnetite within the SAED pattern.

Fig. 6 presents a comparison of the thermogravimetric analysis results for pristine Fe_3O_4 and Fe_3O_4@APTES nanoparticles obtained through two different methods: microwave-assisted silanization of pre-synthesized magnetite nanoparticles and simultaneous on-chip synthesis and silanization of magnetic nanoparticles. Further details on the first two samples can be found in our previous study [13]. However, this image was included to highlight that the fabrication method is an essential factor for the thermal behavior of magnetic nanoparticles, leading to much different results between on-chip functionalization and microwave-assisted process.

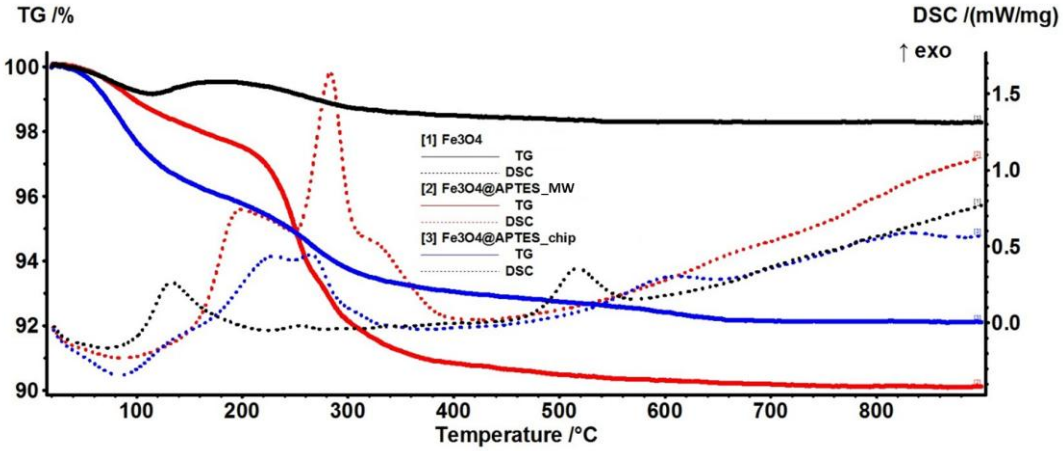

Fig. 6. Thermogravimetric analysis comparison between pristine Fe_3O_4 and Fe_3O_4@APTES NPs (obtained via microwave-assisted synthesis (i.e., "MW") and microfluidic synthesis (i.e., "chip").

The Fe_3O_4@APTES nanoparticles exhibited a mass loss of 4.03% in the temperature range from room temperature to 185°C. The associated endothermic effect, observed with a minimum at 83.7°C, suggests that this mass loss is primarily due to the dehydration process. This is supported by the identification of water and carbon dioxide in the evolved gases (Fig. 7), confirming that water is being eliminated during this phase. Beyond 185°C, an additional mass loss of 3.86% was recorded, accompanied by an exothermic effect with two peaks at 230.1°C and 264.7°C. These peaks correspond to the sequential oxidation of the organic components within the APTES shell.s The main degradation products identified in the evolved gases during this stage are H_2O and CO_2. The gradual mass loss occurring between 350°C and 700°C is attributed to the densification of silica, resulting from the condensation of Si-OH groups [29]. The lack of an

exothermic effect in the 500-600°C range, which is commonly linked to the transformation of maghemite to hematite, suggests that the iron oxide core is effectively shielded from thermal oxidation by the surrounding silica shell [30]. A small exothermic peak at 610.9°C, coupled with a slight presence of CO_2 in the FT-IR 3D diagram, suggests the combustion of residual carbonaceous material. The residual mass after the analysis is 92.10%.

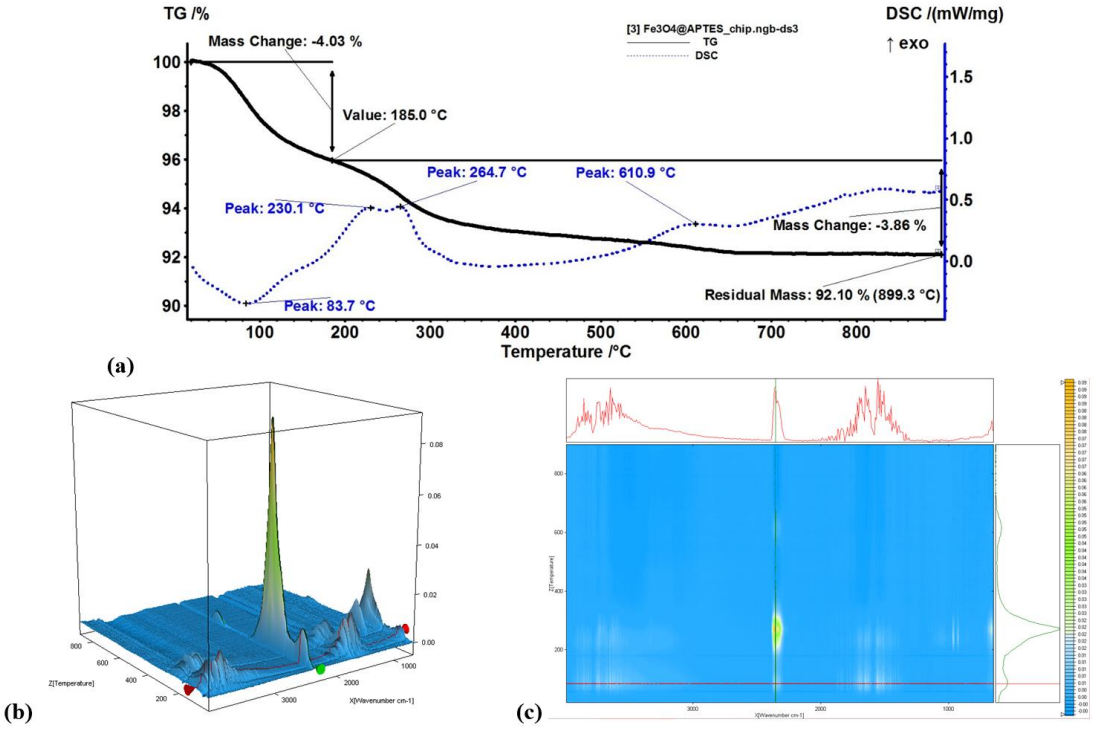

Fig. 7. (a) Thermogravimetric analysis of Fe_3O_4@APTES nanoparticles synthesized on-chip. (b) 3D FT-IR diagram and (c) its 2D projection on the temperature/wavenumber plane, showing the FT-IR spectrum at 82°C (top view) and the trace for CO_2 at 2355 cm^{-1} (right view).

To our knowledge, this is the first time the silanization of iron oxide nanoparticles has been performed on-chip. Several other studies have been conducted on obtaining the same material but following other fabrication approaches [13,24-26,31].

Compared with prior studies in the field, using a single-step microfluidic-assisted co-precipitation and functionalization reaction drastically reduces preparation time, forming Fe_3O_4-APTES NPs in less than 1 minute. Even in comparison with our previous work [13], the synthesis method described in this paper is much more efficient, the elimination of the microwave irradiation stage saving not only the time required for the reaction itself but also the time-

consuming intermediate steps, such as in-between washing, centrifugation, and ultrasonic dispersion.

Moreover, using a 3D microfluidic platform has allowed tight control over reaction parameters and an enhanced mixing of involved reagents, leading to uniform ultra-small products suitable for translation into various future applications (e.g., drug delivery vehicles, nanostructured catalytic materials, and wastewater remediation).

4. Conclusions

This research focused on the concurrent on-chip synthesis and silanization of iron oxide nanoparticles. The approach demonstrated its effectiveness in producing ultra-small, spherical, crystalline, and highly stable Fe_3O_4@APTES nanoparticles, as validated by XRD, DLS, TEM, and SAED characterizations. Additionally, the functionalization of the magnetic cores was confirmed through FT-IR, TEM, and TG-DSC analyses, which verified the successful grafting of the coupling agent onto the nanoparticle surface. Thus, the proposed route for fabricating magnetite nanoparticles covered by an organosilane shell was demonstrated as a fast and reliable method, which, due to the advantages offered by the custom-made 3D microfluidic platform, allowed for achieving uniform core-shell nanoparticles in less time, fewer operating steps, and with lower consumption of chemical reagents.

Acknowledgment

The authors acknowledge the financial support from the European Union (NextGenerationEU) through PNRR.C9-I8: Aerogel-based magnetic nanocomposites for water decontamination (CF 231/29.11.2022). The content of this material does not necessarily represent the official position of the European Union or of the Government of Romania.

R E F E R E N C E S

1. Ganapathe, L.S.; Mohamed, M.A.; Mohamad Yunus, R.; Berhanuddin, D.D. Magnetite (Fe3O4) Nanoparticles in Biomedical Application: From Synthesis to Surface Functionalisation. Magnetochemistry **2020**, 6, doi:10.3390/magnetochemistry6040068.
2. Zhao, X.; Bian, F.; Sun, L.; Cai, L.; Li, L.; Zhao, Y. Microfluidic Generation of Nanomaterials for Biomedical Applications. Small **2020**, 16, 1901943, doi:https://doi.org/10.1002/smll.201901943.

3. Sajid, M.; Płotka-Wasylka, J. Nanoparticles: Synthesis, characteristics, and applications in analytical and other sciences. Microchemical Journal **2020**, 154, 104623, doi:10.1016/j.microc.2020.104623.
4. Lu, X.; Wang, T.; Cao, M.; Cheng, W.; Yang, H.; Xu, H.; He, C.; Tian, L.; Li, Z. Homogeneous NiMoO4–Co(OH)2 bifunctional heterostructures for electrocatalytic oxygen evolution and urea oxidation reaction. International Journal of Hydrogen Energy **2023**, doi:https://doi.org/10.1016/j.ijhydene.2023.04.257.
5. Lu, X.; Du, M.; Wang, T.; Cheng, W.; Li, J.; He, C.; Li, Z.; Tian, L. Ultrafast fabrication of nanospherical CoFe alloys for boosting electrocatalytic water oxidation. International Journal of Hydrogen Energy **2023**, doi:https://doi.org/10.1016/j.ijhydene.2023.05.105.
6. Tian, L.; Liu, Y.; He, C.; Tang, S.; Li, J.; Li, Z. Hollow heterostructured nanocatalysts for boosting electrocatalytic water splitting. The Chemical Record **2023**, 23, e202200213.
7. Ahangaran, F.; Navarchian, A.H. Recent advances in chemical surface modification of metal oxide nanoparticles with silane coupling agents: A review. Advances in Colloid and Interface Science **2020**, 286, 102298, doi:https://doi.org/10.1016/j.cis.2020.102298.
8. Cabeza, V.S. High and efficient production of nanomaterials by microfluidic reactor approaches. In Advances in Microfluidics–New Applications in Biology, Energy, and Materials Sciences; InTech Rijeka: 2016.
9. Prabakar, A.C.; Killivalavan, G.; Sivakumar, D.; Babu, K.C.; Manikandan, E.; Balaraju, M. Exploring Structural, Morphological, and Magnetic Properties of Zinc Nickel Ferrites Systems Nanocomposites. Biointerface research in applied chemistry **2021**, 11, 7785-7793.
10. Moaca, E.A.; Coricovac, E.D.; Soica, C.M.; Pinzaru, I.A.; Pacurariu, C.S.; Dehelean, C.A. Preclinical aspects on magnetic iron oxide nanoparticles and their interventions as anticancer agents: enucleation, apoptosis and other mechanism. Iron Ores Iron Oxide Mater **2018**, 229-254.
11. Niculescu, A.-G.; Chircov, C.; Grumezescu, A.M. Magnetite nanoparticles: Synthesis methods–A comparative review. Methods **2022**, 199, 16-27.
12. Sodipo, B.K.; Aziz, A.A. A sonochemical approach to the direct surface functionalization of superparamagnetic iron oxide nanoparticles with (3-aminopropyl) triethoxysilane. Beilstein journal of nanotechnology **2014**, 5, 1472-1476.
13. Niculescu, A.-G.; Moroșan, A.; Bîrcă, A.C.; Gherasim, O.; Oprea, O.C.; Vasile, B.Ș.; Purcăreanu, B.; Mihaiescu, D.E.; Rădulescu, M.; Grumezescu, A.M. Microwave-Assisted Silanization of Magnetite Nanoparticles Pre-Synthesized by a 3D Microfluidic Platform. Nanomaterials **2023**, 13, doi:10.3390/nano13202795.
14. Schemberg, J.; Abbassi, A.E.; Lindenbauer, A.; Chen, L.-Y.; Grodrian, A.; Nakos, X.; Apte, G.; Khan, N.; Kraupner, A.; Nguyen, T.-H.; et al. Synthesis of Biocompatible Superparamagnetic Iron Oxide Nanoparticles (SPION) under Different Microfluidic Regimes. ACS Applied Materials & Interfaces **2022**, 14, 48011-48028, doi:10.1021/acsami.2c13156.
15. Bezelya, A.; Küçüktürkmen, B.; Bozkır, A. Microfluidic Devices for Precision Nanoparticle Production. Micro **2023**, 3, 822-866, doi:10.3390/micro3040058.
16. Li, Z.; Zhang, B.; Dang, D.; Yang, X.; Yang, W.; Liang, W. A review of microfluidic-based mixing methods. Sensors and Actuators A: Physical **2022**, 344, 113757, doi:https://doi.org/10.1016/j.sna.2022.113757.
17. Mohammadi, M.; Ahmed Qadir, S.; Mahmood Faraj, A.; Hamid Shareef, O.; Mahmoodi, H.; Mahmoudi, F.; Moradi, S. Navigating the future: Microfluidics charting new routes in

drug delivery. International Journal of Pharmaceutics **2024**, 124142, doi:https://doi.org/10.1016/j.ijpharm.2024.124142.

18. Niculescu, A.-G.; Chircov, C.; Bîrcă, A.C.; Grumezescu, A.M. Fabrication and Applications of Microfluidic Devices: A Review. International Journal of Molecular Sciences **2021**, 22, doi:10.3390/ijms22042011.
19. Hamdallah, S.I.; Zoqlam, R.; Erfle, P.; Blyth, M.; Alkilany, A.M.; Dietzel, A.; Qi, S. Microfluidics for pharmaceutical nanoparticle fabrication: The truth and the myth. International Journal of Pharmaceutics **2020**, 584, 119408, doi:https://doi.org/10.1016/j.ijpharm.2020.119408.
20. Niculescu, A.-G.; Mihaiescu, D.E.; Grumezescu, A.M. A Review of Microfluidic Experimental Designs for Nanoparticle Synthesis. International Journal of Molecular Sciences **2022**, 23, doi:10.3390/ijms23158293.
21. Kašpar, O.; Koyuncu, A.H.; Hubatová-Vacková, A.; Balouch, M.; Tokárová, V. Influence of channel height on mixing efficiency and synthesis of iron oxide nanoparticles using droplet-based microfluidics. RSC Advances **2020**, 10, 15179-15189, doi:10.1039/D0RA02470H.
22. Tian, F.; Cai, L.; Liu, C.; Sun, J. Microfluidic technologies for nanoparticle formation. Lab on a Chip **2022**, 22, 512-529.
23. Vasilescu, S.A.; Bazaz, S.R.; Jin, D.; Shimoni, O.; Warkiani, M.E. 3D printing enables the rapid prototyping of modular microfluidic devices for particle conjugation. Applied Materials Today **2020**, 20, 100726, doi:https://doi.org/10.1016/j.apmt.2020.100726.
24. Hosseini, F.; Mirabdullah Seyed, S.; Farhadyar, N. Fe3O4 nanoparticles modified with APTES as the carrier for (+)-(S)-2-(6-methoxynaphthalen-2-yl) propanoic acid (Naproxen) and (RS) 2-(3-benzoylphenyl)-propionic acid (Ketoprofen) drug. Oriental Journal of Chemistry **2014**, 30, 1609-1618, doi:https://doi.org/10.13005/ojc/300420.
25. Villa, S.; Riani, P.; Locardi, F.; Canepa, F. Functionalization of Fe3O4 NPs by Silanization: Use of Amine (APTES) and Thiol (MPTMS) Silanes and Their Physical Characterization. Materials **2016**, 9, doi:10.3390/ma9100826.
26. Feng, J.; Yu, S.; Li, J.; Mo, T.; Li, P. Enhancement of the catalytic activity and stability of immobilized aminoacylase using modified magnetic Fe3O4 nanoparticles. Chemical Engineering Journal **2016**, 286, 216-222.
27. Serrano-Lotina, A.; Portela, R.; Baeza, P.; Alcolea-Rodríguez, V.; Villarroel, M.; Ávila, P. Zeta potential as a tool for functional materials development. Catalysis Today **2023**, 423, 113862.
28. Li, K.; Zhong, W.; Li, P.; Ren, J.; Jiang, K.; Wu, W. Antibacterial mechanism of lignin and lignin-based antimicrobial materials in different fields. International Journal of Biological Macromolecules **2023**, 126281.
29. Petrișor, G.; Motelica, L.; Ficai, D.; Ilie, C.-I.; Trușcă, R.D.; Surdu, V.-A.; Oprea, O.-C.; Mîrț, A.-L.; Vasilievici, G.; Semenescu, A. Increasing bioavailability of trans-ferulic acid by encapsulation in functionalized mesoporous silica. Pharmaceutics **2023**, 15, 660.

30. Chircov, C.; Matei, M.-F.; Neacșu, I.A.; Vasile, B.S.; Oprea, O.-C.; Croitoru, A.-M.; Trușcă, R.-D.; Andronescu, E.; Sorescu, I.; Bărbuceanu, F. Iron oxide–silica core–shell nanoparticles functionalized with essential oils for antimicrobial therapies. Antibiotics **2021**, 10, 1138.

31. Sahoo, J.K.; Paikra, S.K.; Baliarsingh, A.; Panda, D.; Rath, S.; Mishra, M.; Sahoo, H. Surface functionalization of graphene oxide using amino silane magnetic nanocomposite for Chromium (VI) removal and bacterial treatment. Nano Express **2020**, 1, 010062.